



This open access document is published as a preprint in the Beilstein Archives with doi: 10.3762/bxiv.2019.57.v1 and is considered to be an early communication for feedback before peer review. Before citing this document, please check if a final, peer-reviewed version has been published in the Beilstein Journal of Nanotechnology.

This document is not formatted, has not undergone copyediting or typesetting, and may contain errors, unsubstantiated scientific claims or preliminary data.

Preprint Title Dynamics of superparamagnetic nanoparticle in viscous liquid in rotating magnetic field

Authors Nikolai A. Usov, Ruslan A. Rytov and Vasilii A. Bautin

Article Type Full Research Paper

Supporting Information File 1 SupplMaterial.pptx; 3.2 MB

ORCID® iDs Nikolai A. Usov - <https://orcid.org/0000-0002-2061-3467>; Ruslan A. Rytov - <https://orcid.org/0000-0002-7963-3673>

License and Terms: This document is copyright 2019 the Author(s); licensee Beilstein-Institut.

This is an open access publication under the terms of the Creative Commons Attribution License (<http://creativecommons.org/licenses/by/4.0>). Please note that the reuse, redistribution and reproduction in particular requires that the author(s) and source are credited.

The license is subject to the Beilstein Archives terms and conditions: <https://www.beilstein-archives.org/xiv/terms>.

The definitive version of this work can be found at: doi: <https://doi.org/10.3762/bxiv.2019.57.v1>

Dynamics of superparamagnetic nanoparticle in viscous liquid in rotating magnetic field

Nikolai A. Usov*^{1,2}, Ruslan A. Rytov¹, Vasilij A. Bautin¹

¹National University of Science and Technology «MISIS», 119049, Moscow, Russia

²Pushkov Institute of Terrestrial Magnetism, Ionosphere and Radio Wave Propagation, Russian Academy of Sciences, IZMIRAN, 108480, Troitsk, Moscow, Russia

Abstract. The dynamics of magnetic nanoparticle in a viscous liquid in rotating magnetic field has been studied by means of numerical simulation and analytical calculations. In the magneto-dynamics approximation three different modes of motion of the unit magnetization vector and particle director are distinguished depending on the rotating magnetic field frequency and amplitude. The specific absorption rate of a dilute assembly of superparamagnetic nanoparticles in rotating magnetic field is calculated by solving the Landau – Lifshitz stochastic equation for unit magnetization vector and stochastic equation for particle director. At elevated frequencies an optimal range of particle diameters is found where the specific absorption rate of an assembly in rotating magnetic field has a maximum. It is shown that for magnetic hyperthermia in rotating magnetic field it is preferable to use rotating magnetic fields of moderate amplitude, $H_0 = 100$ Oe, in the frequency range 400-600 kHz.

PACS: 75.20.-g; 75.50.Tt; 75.40.Mg

Keywords: Magnetic nanoparticles; Viscous liquid; Rotating magnetic field; Magnetic hyperthermia; Specific absorption rate; Numerical simulation

E-mail: usov@obninsk.ru (Nikolai A. Usov, corresponding author)

Introduction

Magnetic nanoparticles are promising for various areas of biomedicine [1-4], such as magnetic resonance imaging [5-7], targeted drug delivery [8-10], magnetic hyperthermia [11-20], etc. Iron oxide nanoparticles are most frequently used in biomedicine due to their biocompatibility, biodegradability and relatively high saturation magnetization. In magnetic hyperthermia [2,3,11-20], magnetic nanoparticles are directly introduced into tumor and are exposed to an alternating magnetic field (AMF) of frequency $f = 100 - 500$ kHz and amplitude $H_0 = 100 - 200$ Oe. This allows one to maintain the temperature of the tumor about 42 C by absorbing the alternating magnetic field energy. According to a number of medical indications [1,3,19,20], the certain thermal effect in combination with radiotherapy or chemotherapy can significantly improve the results of cancer treatment.

One of the main technological problems of current magnetic hyperthermia development stage is the optimal choice of sizes and magnetic parameters of nanoparticles, as well as the selection of appropriate AMF frequency and amplitude. Besides, a biological environment of an assembly of magnetic nanoparticles may be different in a human body[1-3]. In most cases magnetic nanoparticles penetrate directly into the tumor cells, or surrounding tissues [2, 3]. Inside the cell magnetic nanoparticles form usually dense clusters tightly bound to the surrounding tissues [21–24], so that the rotation of a nanoparticle as a whole in AMF is difficult, or completely absent. Thus, the absorption of the AMF energy is only associated with the dynamics of the particle magnetic moments. However, if nanoparticles remain distributed in biological fluids (blood, serum), the intensity of AMF energy absorption is determined also by the rotation of the nanoparticles as a whole in a viscous liquid [25,26].

Various mathematical approaches are necessary for a theoretical description of these processes. While in dense nanoparticle assemblies that are tightly bound to surrounding tissues the mechanical rotation of the particles is inhibited, one has to take into account the influence of strong magnetic-dipole interaction between nanoparticles [27–32] on the energy absorption intensity. On the other hand, for particles distributed in a viscous liquid it is necessary to take into account [25] a coupled motion of the unit magnetization vector $\vec{\alpha}$ and nanoparticle director \vec{n} that is parallel to the direction of the easy anisotropy axis of a rotating nanoparticle.

Recently, the application of a rotating magnetic field (RMF) in biomedicine, in particular in magnetic hyperthermia, has been studied both theoretically [33–39] and experimentally [40–43]. Unfortunately, the specific absorption rate (SAR) measured in the RMF [41,43] for assembly of particles distributed in a viscous liquid turned out to be very small, of the order of a few watts per gram. At the same time, the SAR of an assembly of superparamagnetic nanoparticles in AMF under the optimal conditions reaches the values of the order of several hundred watts per gram [3, 15-18]. It is possible that the geometric and magnetic parameters of the particles used in the experiments [41,43]

were far from optimal. Therefore, it is important to determine the optimal geometric and magnetic parameters of the nanoparticles, as well as the amplitudes and frequencies, at which the SAR of the superparamagnetic nanoparticle assembly in RMF will be large enough to be used in magnetic hyperthermia.

In this work the detailed numerical calculations of the SAR in RMF for a dilute assembly of superparamagnetic particles with uniaxial anisotropy distributed in a viscous liquid have been carried out. First, the behavior of a magnetic particle in RMF is studied in the magneto-dynamics approximation [25,44,45], neglecting the thermal fluctuations of the particle magnetic moment and particle director. On the plane of parameters (f, H_0) three domains for different modes of motion of the unit magnetization vector and particle director are distinguished. The boundaries between these domains, first determined numerically, are then confirmed by analytical calculations.

Then, the SAR of a dilute assembly of superparamagnetic nanoparticles in a RMF is calculated by solving the Landau – Lifshitz stochastic equation for unit magnetization vector and stochastic equation for particle director. It is shown that at elevated frequencies, $f > 100$ kHz, there is an optimal range of particle diameters where the SAR in RMF has a maximum. This behavior of the SAR resembles that in AMF, [11,25]. For iron oxide nanoparticles of optimal diameters the SAR in RMF reaches the values of the order of 400 – 450 W/g at a frequency $f = 400$ kHz and moderate amplitude, $H_0 = 100$ Oe. It is important to note that for sufficiently large particle diameters the SAR in RMF is approximately 2 times larger than that in AMF.

Magneto-dynamics approximation

Let us consider first the dynamics in a viscous liquid of a spherical single-domain nanoparticle of a sufficiently large diameter, close to the single-domain one. In this case one can neglect the influence of thermal fluctuations of the behavior of magnetic moment and the director of the particle and describe their movement in RMF in the magneto-dynamics approximation [25,44,45]. Without loss of generality, one can assume that the magnetic field of constant frequency f and amplitude H_0 rotates in the XY plane of the Cartesian coordinates, so that

$$\vec{H}_0(t) = (H_0 \cos(\omega t), H_0 \sin(\omega t), 0). \quad (1)$$

Neglecting weak magnetic damping and a small moment of inertia of a magnetic nanoparticle, the magneto-dynamic equations of motion of the unit vectors $\vec{\alpha}$ and \vec{n} in a viscous fluid have the form [25]

$$\frac{\partial \vec{n}}{\partial t} = G(\vec{\alpha}\vec{n})(\vec{\alpha} - \vec{n}(\vec{\alpha}\vec{n})); \quad (2)$$

$$\frac{\partial \vec{\alpha}}{\partial t} = -\gamma(\vec{\alpha} \times \vec{H}_0(t)) - \gamma H_k(\vec{\alpha}\vec{n})(\vec{\alpha} \times \vec{n}), \quad (3)$$

where $G = K/3\eta$, η is the the liquid viscosity, K is the effective magnetic anisotropy constant of the nanoparticle, $H_k = 2K/M_s$ is the particle anisotropy field, and M_s is the saturation magnetization.

Eqs. (1) - (3) describe the complex coupled dynamics of unit vectors $\vec{\alpha}$ and \vec{n} in RMF. Numerical solution of Eqs. (1) - (3) with a small time step following the procedure described earlier [25] reveals three stationary modes of motion of the vectors $\vec{\alpha}$ and \vec{n} as a function of the RMF frequency and amplitude. Figures 1a, 1b show the regular dynamics of the vector $\vec{\alpha}$ in the first and second modes of particle motion, respectively. The director of the particle moves in these modes in a similar way, but it has a constant time shift with respect to vector $\vec{\alpha}$. The dynamics of the vectors $\vec{\alpha}$ and \vec{n} in the third mode of particle motion is shown in Figures 1c, 1d, respectively. The illustrative calculations were performed for magnetic nanoparticles of iron oxide, with a saturation magnetization $M_s = 350 \text{ emu/cm}^3$, magnetic anisotropy constant $K = 10^5 \text{ erg/cm}^3$. The liquid viscosity is assumed to be $\eta = 0.01 \text{ g/(cm}\times\text{s)}$.

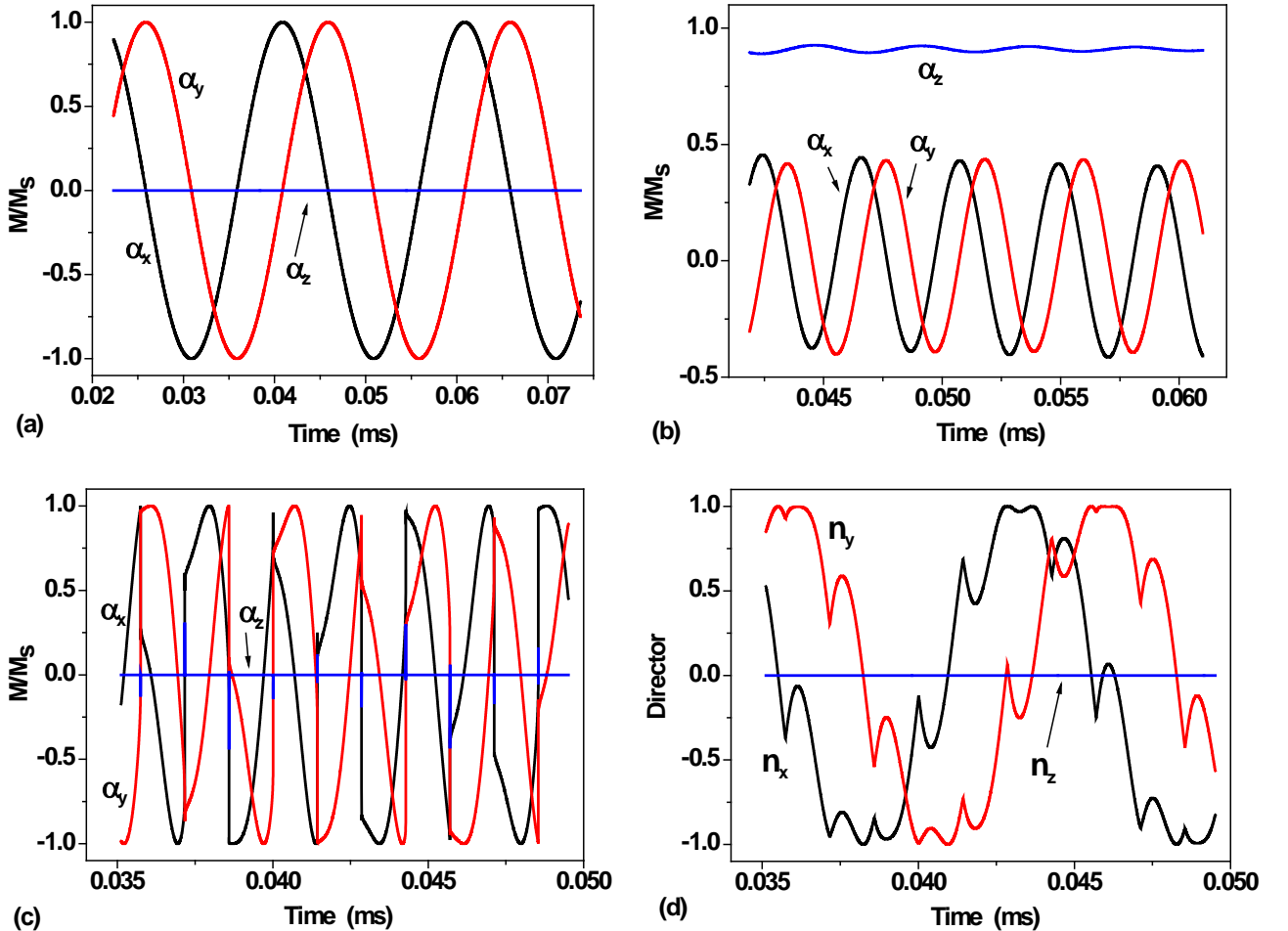


Figure 1: Dynamics of the unit magnetization vector in RMF in the magneto-dynamics approximation for various regimes of stationary motion of a nanoparticle in a viscous liquid: a) first mode, $f = 50 \text{ kHz}$, $H_0 = 200 \text{ Oe}$; b) second mode, $f = 240 \text{ kHz}$, $H_0 = 100 \text{ Oe}$; c) and d) particle dynamics in the third mode, $f = 450 \text{ kHz}$, $H_0 = 400 \text{ Oe}$.

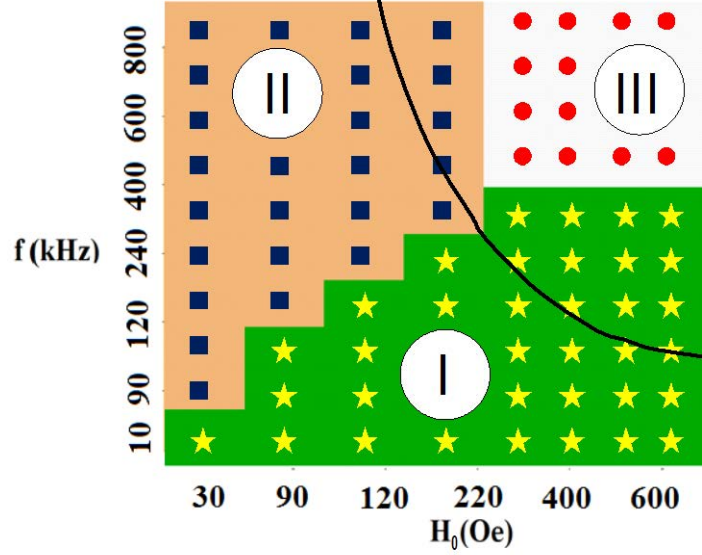


Figure 2: The domains of various magneto- dynamic modes of motion of a superparamagnetic nanoparticle in a viscous liquid depending on the RMF frequency and amplitude. The Brezovich area [46,47], recommended for medical reasons for use in magnetic hyperthermia, $fH_0 \leq 6.25 \times 10^4$ kHz*Oe, is located below the black curve.

The domains of existence of various magneto- dynamic regimes I – III on the plane (f, H_0) determined numerically at the above mentioned physical parameters are shown in Figure 2. Different symbols in this figure show the specific pairs of the parameters (f, H_0) for which numerical calculations were performed. The area below the black curve in Figure 2, corresponds to the condition $fH_0 \leq 6.25 \times 10^4$ kHz*Oe. This domain of applied magnetic field frequencies and amplitudes is recommended for medical reasons for use in magnetic hyperthermia [46,47].

In the first mode existing in the domain I in Figure 2, at low and moderate RMF frequencies, the vectors $\vec{\alpha}$ and \vec{n} rotate in unison around the Z axis with the RMF frequency. However, there are constant phase differences between the vectors $\vec{\alpha}$ and \vec{n} , and the magnetic field vector, respectively. At the same time, Z - components of the vectors $\vec{\alpha}$ and \vec{n} in the domain I are close to zero, so that the rotation of these vectors occurs in fact near the XY plane. An example of such a motion for unit magnetization vector $\vec{\alpha}$ is shown in Figure 1a.

In the second mode existing in the domain II in Figure 2, both vectors go out of the XY plane, so that they have significant components parallel to the Z axis. An example of motion of the unit magnetization vector in the domain II is shown in Figure 1b. The vector \vec{n} moves in the domain II similarly. Projections of the vectors $\vec{\alpha}$ and \vec{n} on the XY plane have a constant phase differences between themselves and with the magnetic field vector.

Finally, in the third mode existing in the domain III in Figure 2, the vectors $\vec{\alpha}$ and \vec{n} return to the plane of magnetic field rotation, but they move in this plane with different average frequencies.

The unit magnetization vector gradually lags behind the magnetic field vector and periodically jumps from one magnetic potential well to another. Such behavior of the unit magnetization vector components is shown in Figure 1c. As Figure 1d shows, the director of the particle also rotates around the Z axis with a reduced average frequency. When the vector $\vec{\alpha}$ jumps, it experiences complex oscillatory movement.

To confirm the features of the particle magneto - dynamics in RMF obtained numerically and to extend these results to a wide range of physical parameters, we also carried out in Appendix an analytical analysis of the Eqs. (1) - (3). The analytical solution constructed in Appendix describes the behavior of vectors $\vec{\alpha}$ and \vec{n} in the domains I and II on the plane of parameters (f, H_0) , shown in Figure 2.

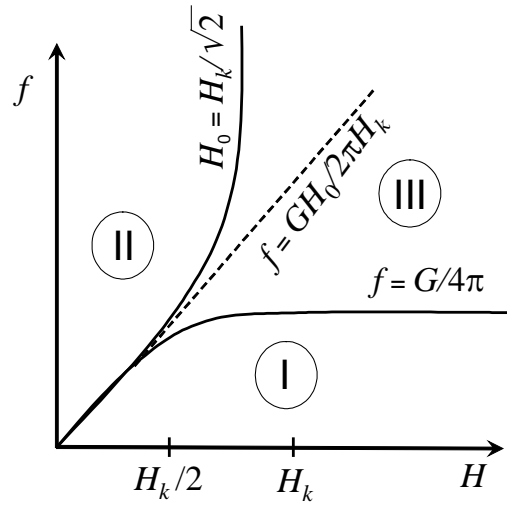


Figure 3: The domains I – III of various magneto- dynamic modes of nanoparticle motion in a viscous liquid in RMF, obtained analytically based on equations (1) - (3) (see Appendix).

The boundaries between the domains I – III of various magneto- dynamic modes of particle motion in viscous liquid in RMF, obtained as a result of analysis of the nonlinear system of equations investigated in Appendix, are shown in Figure 3. The obtained analytical results are in excellent agreement with the numerically defined regions of the existence of these modes shown in Figure 2 for specific values of M_s , K and η .

SAR in RMF

We now turn to the SAR calculation for a dilute assembly of superparamagnetic nanoparticles in RMF, taking into account thermal fluctuations of the magnetic moment and the director of a superparamagnetic nanoparticle. The SAR calculations were carried out by solving jointly the Landau – Lifshitz stochastic equation for unit magnetization vector and the stochastic equation for the director of a superparamagnetic nanoparticle.

The stochastic Landau – Lifshitz equation for the unit magnetization vector of the particle has the form [48-51]

$$\frac{\partial \vec{\alpha}}{\partial t} = -\gamma_1 \vec{\alpha} \times (\vec{H}_{ef} + \vec{H}_{th}) - \kappa \gamma_1 \vec{\alpha} \times (\vec{\alpha} \times (\vec{H}_{ef} + \vec{H}_{th})), \quad (4)$$

where $\gamma_1 = |\gamma|/(1+\kappa^2)$, κ is the phenomenological damping parameter, $\vec{H}_{ef} = \vec{H}_0 + H_k(\vec{\alpha}\vec{n})\vec{n}$, and \vec{H}_{th} is the random thermal magnetic field that causes thermal fluctuations of the particle magnetic moment. The stochastic equation for the nanoparticle director is given by [25,51,52]

$$\frac{\partial \vec{n}}{\partial t} = G(\vec{\alpha}\vec{n})(\vec{\alpha} - (\vec{\alpha}\vec{n})\vec{n}) - \frac{1}{\xi}[\vec{n}, \vec{N}_{th}], \quad (5)$$

where $\xi = 6\eta V$ is the friction coefficient of a particle in a viscous liquid, and \vec{N}_{th} is the fluctuating rotational moment, which describes the free Brownian rotational motion of a particle in a liquid in the absence of external magnetic field.

In accordance with the fluctuation-dissipation theorem [51], the components of the fluctuating rotational moment satisfy the statistical relations [52], ($i, j = x, y, z$)

$$\langle N_{th,i}(t) \rangle = 0; \quad \langle N_{th,i}(t) N_{th,j}(t_1) \rangle = 2k_B T \xi \delta_{ij} \delta(t - t_1), \quad (6)$$

where k_B is the Boltzmann constant, T is the absolute temperature, $\delta_{\alpha\beta}$ is the Kronecker's symbol, and $\delta(t)$ is the delta function. For the components of the fluctuating thermal magnetic field there are similar statistical relations [48]

$$\langle H_{th,i}(t) \rangle = 0; \quad \langle H_{th,i}(t) H_{th,j}(t_1) \rangle = \frac{2k_B T \kappa}{|\gamma_0| M_s V} \delta_{ij} \delta(t - t_1). \quad (7)$$

The SAR of a dilute assembly of superparamagnetic nanoparticles in magnetic field rotating at a frequency f in the XY plane is determined by the integral

$$SAR = \frac{f M_s}{\rho} \oint (\langle \alpha_x \rangle dH_x + \langle \alpha_y \rangle dH_y), \quad (8)$$

where ρ is the nanoparticle density. The averaged components of the unit magnetization vector $\langle \alpha_x \rangle$ and $\langle \alpha_y \rangle$ are calculated by solving stochastic equations (4) - (7) and averaging the results over a sufficiently large number of independent numerical experiments carried out with the same magnetic nanoparticle under arbitrary initial conditions.

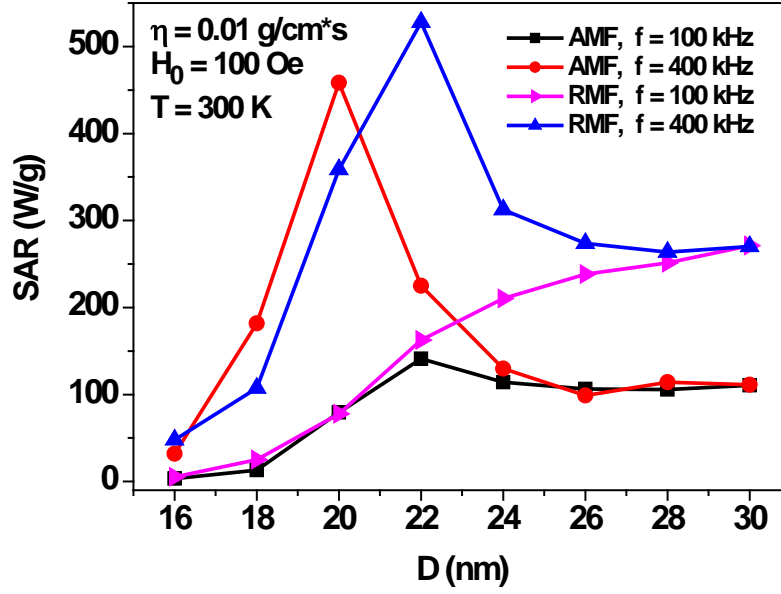


Figure 4: Comparison of the SAR of a dilute assembly of superparamagnetic nanoparticles in AMF and RMF depending on the nanoparticle diameter for two frequencies, $f = 100$ and 400 kHz, at a fixed magnetic field amplitude, $H_0 = 100$ Oe.

First of all, it is interesting to compare the results of the SAR calculation of a dilute assembly of superparamagnetic nanoparticles distributed in a viscous fluid in RMF and AMF, respectively. In the calculations presented in Figure 4, the saturation magnetization of nanoparticles is given by $M_s = 350$ emu/cm³, the effective magnetic anisotropy constant $K = 10^5$ erg/cm³, the particle density $\rho = 5$ g/cm³, the viscosity of the liquid $\eta = 0.01$ g/(cm×s), the magnetic damping constant is assumed to be $\kappa = 0.1$, medium temperature $T = 300$ K.

As Figure 4 shows, for a dilute assembly of superparamagnetic nanoparticles in RMF SAR monotonously increases with increasing particle diameter at a moderate frequency, $f = 100$ kHz. However, with an increase in the frequency, $f = 400$ kHz, a rather narrow region of optimal nanoparticle diameters appears, $D = 20 - 24$ nm, in which the SAR reaches its maximum values. The behavior of SAR depending on the nanoparticle diameter in AMF is similar. However, it is important to note that as Figure 4 shows, in the range of particle diameters $D > 24$ nm the SAR in RMF is approximately 2 times larger than that in AMF.

For completeness, we also calculated SAR in RMF for assemblies of superparamagnetic nanoparticles with different magnetic anisotropy constants, and in liquids of different viscosities. As Figure 5a shows, with a slight decrease in the magnetic anisotropy constant, the dependence of SAR on the average nanoparticle diameter does not change appreciably, but the SAR maximum shifts to larger particle diameters. Figure 5b shows the dependence of SAR on the average diameter of nanoparticles in liquids of various viscosities.

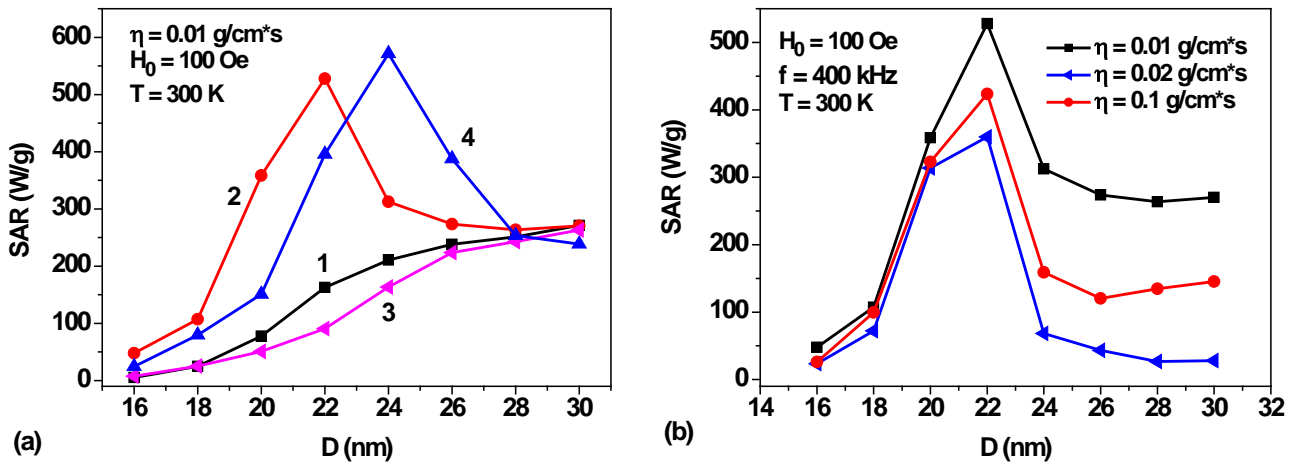


Figure 5: a) SAR in RMF for dilute assemblies of superparamagnetic nanoparticles with various magnetic anisotropy constants: 1) $K = 10^5 \text{ erg/cm}^3$, $f = 100 \text{ kHz}$, 2) $K = 10^5 \text{ erg/cm}^3$, $f = 400 \text{ kHz}$, 3) $K = 8 \times 10^4 \text{ erg/cm}^3$, $f = 100 \text{ kHz}$, 4) $K = 8 \times 10^4 \text{ erg/cm}^3$, $f = 400 \text{ kHz}$. b) SAR of assembly of superparamagnetic nanoparticles depending on the liquid viscosity.

One can see in this figure that the range of optimal particle diameters varies little in the range of $\eta = 0.01 - 0.1 \text{ g/(cm}^2\text{s)}$, but SAR decreases with increasing viscosity, especially in the region of relatively large nanoparticle diameters.

Results and discussion

The results of numerical simulations presented in Figures 4, 5 show that with an optimal choice of the particle diameters sufficiently large SAR values, of the order of 400–500 W/g can be obtained in RMF at frequency $f = 400 \text{ kHz}$ and moderate amplitude, $H_0 = 100 \text{ Oe}$. Nevertheless, the experimentally measured [41,43] SAR values in RMF for an assembly of iron oxide nanoparticles distributed in a viscous liquid turned out to be very small, only about 1.0 - 4.0 W/g. This may be due to the small RMF amplitudes used in experiments [41,43]. Indeed, in Ref. 43 the SAR values of the assembly in RMF were measured in a fairly wide frequency range, from 100 to 800 kHz. However, the RMF amplitude was only 1 or 2 kA/m, that is, it did not exceed 25 Oe. As our numerical simulations show, it is impossible to obtain noticeable SAR values with such small RMF amplitude. In Ref. 41 the SAR measurements were carried out at moderate frequencies, $f = 130$ and 160 kHz , but the RMF amplitude was higher, $H_0 = 4.1 \text{ kA/m}$. However, in this case the measured SAR values [41] turned out to be also small, of the order of 1 W/g. One can see in Figure 6 that the numerical simulations performed at the same RMF frequency and amplitude predict an order of magnitude larger SAR values than that measured in Ref. 41.

It should be noted however that the numerical calculations presented in Figure 6 are carried out for an assembly of nanoparticles with a diameter $D = 20$ nm. This diameter is close to the optimal diameter for particles with typical magnetic parameters of iron oxide, that is, $M_s = 350$ emu/cm³, $K = 10^5$ erg/cm³, $\rho = 5$ g/cm³. Therefore, one can assume that the small SAR values measured in [41] are related to the fact that the average particle diameter in this experiment was far from the optimal one, $D \approx 20 - 24$ nm. On the other hand, the calculated SAR values in RMF turned out to be slightly higher than the corresponding SAR values in AMF, in agreement with the results obtained in Refs. 41, 43.

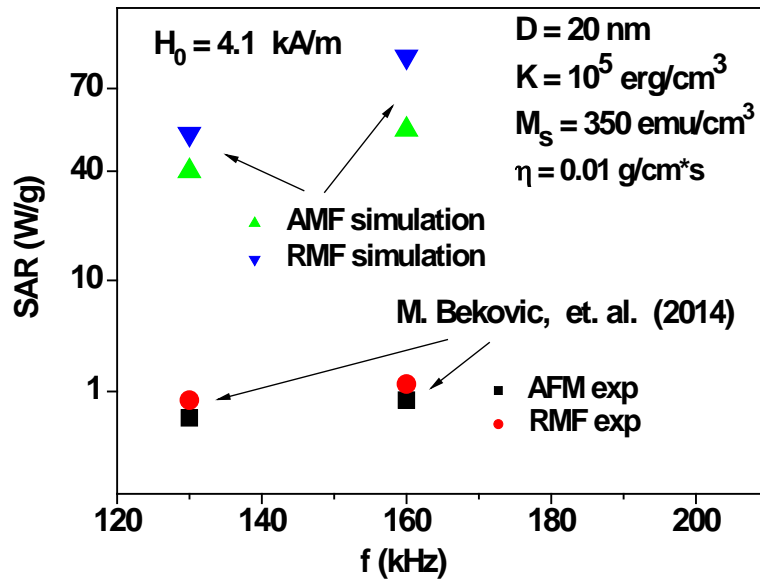


Figure 6: Comparison of the experimentally measured [41] SAR values at frequencies $f = 130, 160$ kHz and amplitude $H_0 = 4.1$ kA/m, with the SAR calculated numerically for a dilute assembly of magnetic nanoparticles in AMF and RMF, respectively.

The numerical results obtained show that in order to achieve sufficiently high SAR values in magnetic hyperthermia, great attention should be paid to the proper choice of magnetic and geometrical parameters of nanoparticles, as well as the selection of the appropriate RMF frequency and amplitude. It is worth noting that frequencies, $f = 130, 160$ kHz, and amplitude, $H_0 = 4.1$ kA/m, investigated in Figure 6 correspond to domain I in the diagram of Figure 2. Due to moderate SAR values obtained numerically, this set of parameters is not suitable for magnetic hyperthermia. In order to determine the optimal RMF frequency and amplitude we calculated the SAR at various points in the diagram of Figure 2, taking into account the weaker Brezovich criterion [47], $fH_0 \leq 6.25 \times 10^4$ kHz*Oe.

As Figure 2 shows, in the Brezovich domain there are I and II magneto- dynamic modes of nanoparticle motion in RMF. In this connection, it is interesting to investigate which type of particle magneto- dynamics is preferable for use in magnetic hyperthermia. To answer this question, we performed SAR calculations for a dilute assembly of magnetic nanoparticles in RMF in two

characteristic cases: a) at a given frequency, $f = 120$ kHz, in the range of amplitudes $H_0 = 50 - 550$ Oe, and b) at given field amplitude, $H_0 = 120$ Oe, in the frequency range $f = 50 - 1050$ kHz. The calculations were performed for dilute assemblies of iron oxide nanoparticles with characteristic diameters $D = 16, 20, 30$ nm. The liquid viscosity was taken to be $\eta = 0.01$ g/(cm \times s), the medium temperature being $T = 300$ K.

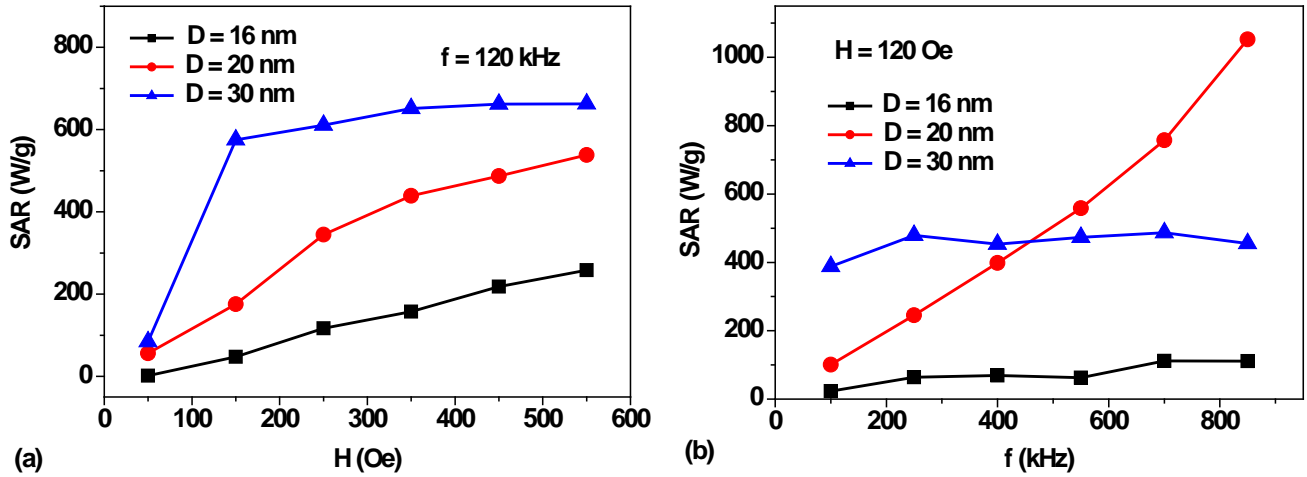


Figure 7: a) SAR of a dilute assembly of iron oxide nanoparticles of different diameters at fixed frequency, $f = 120$ kHz, depending on the RMF amplitude; b) the same for fixed RMF amplitude, $H_0 = 120$ Oe, depending on the field frequency.

As Figure 7a shows, at a fixed frequency, $f = 120$ kHz, SAR increases with increasing particle diameter, or RMF amplitude. However, for nanoparticles of the maximum investigated diameter, $D = 30$ nm, the increase in SAR in the field interval $H_0 = 150 - 500$ Oe is insignificant. In addition, the use of variable magnetic fields of large amplitude requires the generation of strong electric currents, which may be unsafe in a medical clinic. In this regard, it seems more promising to use in magnetic hyperthermia RMF of moderate amplitude, $H_0 = 100 - 120$ Oe, but at frequencies of about 400 - 600 kHz. As Figure 7b shows, in this case SAR values of about 400–600 W/g can be obtained in a wide range of nanoparticle diameters, $D = 20$ –30 nm.

Conclusions

In this paper, the dynamics of a superparamagnetic nanoparticle in a viscous fluid in RMF is studied using both numerical simulation and analytical calculations. This topic has recently attracted considerable interest [33–43] in view of the possibility of using magnetic nanoparticles in magnetic hyperthermia for the cancer treatment. Unfortunately, in experiments [41,43] very small SAR values, of the order of several watts per gram, have been measured in RMF for assembly of superparamagnetic nanoparticles distributed in a viscous liquid. However, the geometrical and magnetic parameters of the

particles used in the experiments [41,43] were likely to be far from optimal values. Indeed, as Figures 4, 5 show, for nanoparticles of iron oxides very small SAR values should be observed if the particle diameter falls within the range of sizes $D \leq 16$ nm. In addition, RMF of rather small amplitude has been used in these experiments.

Using numerical simulation we determine the optimal particle diameters, as well as the RMF frequencies and amplitudes, at which the SAR of the assembly is large enough for application in magnetic hyperthermia. First of all, for a dilute assembly of superparamagnetic nanoparticles it is shown that at sufficiently high RMF frequencies there is an optimal range of particle diameters where the SAR of the assembly reaches maximum. In addition, sufficiently large theoretical SAR values are obtained in the RMF. They exceed the SAR values in the AMF at the same frequency and field amplitude. For example, for iron oxide nanoparticles of optimal diameters, $D = 20 - 24$ nm, SAR in RMF reaches the values 400 – 450 W/g at frequency $f = 400$ kHz and moderate amplitude $H_0 = 100$ Oe. It is important to note also that in the diameter range $D > 24$ nm the SAR in RMF is approximately 2 times larger than that in AMF. For magnetic hyperthermia in RMF it is preferable to use magnetic fields of moderate amplitude, $H_0 = 100$ Oe, in the frequency range 400-600 kHz. In this case one can obtain the SAR values of the order of 400 - 600 W/g in a wide range of particle diameters, $D = 20 - 30$ nm.

References

1. Pankhurst, Q. A.; Thanh, N. K. T.; Jones S. K.; Dobson, J. *J. Phys. D: Appl. Phys.* **2009**, 42, 224001. doi: 10.1088/0022-3727/42/22/224001
2. Dutz, S.; Hergt, R. *Int. J. Hyperthermia.* **2013**, 29, 790-800. doi: 10.3109/02656736.2013.822993
3. Périgo, E. A.; Hemery, G.; Sandre, O.; Ortega, D.; Garaio, E.; Plazaola, F.; Teran, F. J. *Applied Physics Review.* **2015**, 2, 041302. doi: 10.1063/1.4935688
4. Kolosnjaj-Tabi, J.; Lartigue, L.; Javed, Y.; Luciani, N.; Pellegrino, T.; Wilhelm, C.; Alloyeau, D.; Gazeau, F. *Nano Today.* **2016**, 11, 280 - 284. doi: 10.1016/j.nantod.2015.10.001
5. Saritas, E. U.; Goodwill, P.W.; Croft, L.R.; Konkle, J. J.; Lu, K.; Zheng, B.; Conolly, S. M. *J. Magn. Reson.* **2013**, 229, 116–126. doi: 10.1016/j.jmr.2012.11.029
6. Panagiotopoulos, N.; Duschka, R.L.; Ahlborg, M.; Bringout, G; Debbeler, C.; Graeser, M.; Kaethner, C.; Lüdtke-Buzug, K.; Medimagh, H.; Stelzner, J.; Buzug, T.M.; Barkhausen, J.; Vogt, F.; Haegele, J. *International Journal of Nanomedicine* **2015**, 10, 3097-3114. doi: 10.2147/IJN.S70488
7. Wu, L. C.; Zhang, Y.; Steinberg, G.; Qu, H.; Huang, S.; Cheng, M.; Bliss, T.; Du, F.; Rao, J.; Song, G. *American Journal of Neuroradiology* **2019**, 40, 206–212. doi:10.3174/ajnr.a5896
8. Carregal-Romero, S.; Guardia, P.; Yu, X.; Hartmann, R.; Pellegrino, T.; Parak, W. J. *Nanoscale* **2015**, 7, 570–576. doi:10.1039/c4nr04055d

9. Xin, Y.; Yin, M.; Zhao, L.; Meng, F.; Luo, L. *Cancer Biology & Medicine* **2017**, 14, 228. doi:10.20892/j.issn.2095-3941.2017.0052
10. El-Boubbou, K. *Nanomedicine* **2018**, 13, 953–971. doi:10.2217/nmm-2017-0336
11. Usov, N. A. *J. Appl. Phys.* **2010**, 107, 123909. doi: 10.1063/1.3445879
12. Guardia, P.; Di Corato, R.; Lartigue, L.; Wilhelm, C.; Espinosa, A.; Garcia-Hernandez, M.; Gazeau, F.; Manna, L.; Pellegrino, T. *ACS Nano* **2012**, 6, 3080–3091. doi: 10.1021/nn2048137
13. Martinez-Boubeta, C.; Simeonidis, K.; Makridis, A.; Angelakeris, M.; Iglesias, O.; Guardia, P.; Cabot, A.; Yedra, L.; Estradé, S.; Peiró, F.. *Sci. Reports* **2013**, 3, 1652. doi: 10.1038/srep01652
14. Di Corato, R.; Espinosa, A.; Lartigue, L.; Tharaud, M.; Chat, S.; Pellegrino, T.; Ménager, C.; Gazeau, F.; Wilhelm, C. *Biomaterials* **2014**, 35, 6400–6411. doi: 10.1016/j.biomaterials
15. Materia, M. E.; Guardia, P.; Sathya, A.; Leal, M. P.; Marotta, R.; Di Corato, R.; Pellegrino, T. *Langmuir* **2015**, 31, 808 – 816. doi: 10.1021/la503930s
16. Blanco-Andujar, C.; Ortega, D.; Southern, P.; Pankhurst, Q. A.; Thanh, N. T. K. *Nanoscale* **2015**, 7, 1768 – 1775. doi: 10.1039/c4nr06239f
17. Conde-Leboran, I.; Baldomir, D.; Martinez-Boubeta, C.; Chubykalo-Fesenko, O.; Morales, M. D.; Salas, G.; Cabrera, D.; Camarero, J.; Teran, F. J.; Serantes, D. *J. Phys. Chem. C* **2015**, 119, 15698-15706. doi: 10.1021/acs.jpcc.5b02555
18. Sanz, B.; Calatayud, M. P.; Biasi, E. D.; Lima Jr., E.; Mansilla, M. V.; Zysler, R. D.; Ibarra, M. R.; Goya, G. F. *Sci. Reports* **2016**, 6, 38733. doi: 10.1038/srep38733
19. Kobayashi, T. *Biotechnol. J.* **2011**, 6, 1342–1347. doi: 10.1002/biot.201100045
20. Johannsen, M.; Thiesen, B.; Wust, P.; Jordan A. *Int. J. Hyperthermia*, **2010**; 26, 790–795. doi: 10.3109/02656731003745740
21. Etheridge, M. L.; Hurley, K. R.; Zhang, J.; Jeon, S.; Ring, H. L.; Hogan, C.; Haynes, C. L.; Garwood, M.; Bischof, J. C. *Technology* **2014**, 2, 214 – 228. doi: 10.1142/S2339547814500198
22. Jeon, S.; Hurley, K. R.; Bischof, J. C.; Haynes, C. L.; Hogan, Jr, C. J. *Nanoscale* **2016**, 8, 16053-16064. doi: 10.1039/c6nr04042j
23. Martinez-Boubeta, C.; Simeonidis, K.; Serantes, D.; Leboran, I. C.; Kazakis, I.; Sefanou, G.; Pena, L.; Galceran, R.; Balcells, L.; Monty, C.; Baldomir, D.; Mitrakas, M.; Angelakeris, M. *Adv. Funct. Mater.* **2012**, 22, 3737-3744. doi: 10.1002/adfm.201200307
24. Branquinho, L. C.; Carriao, M. S.; Costa, A. S.; Zufelato, N.; Sousa, M. H.; Miotto, R.; Ivkov, R.; Bakuzis, A. F. *Sci. Reports* **2013**, 3, 2887. doi: 10.1038/srep02887
25. Usov, N. A.; Liubimov, B. Y. *J. Appl. Phys.* **2012**, 112, 023901. doi: 10.1063/1.4737126
26. Cabrera, D.; Lak, A.; Yoshida, T.; Materia, M. E.; Ortega, D.; Ludwig, F.; Guardia, P.; Sathya, A.; Pellegrino, T.; Teran, F. J. *Nanoscale* **2017**, 9, 5094–5101. doi:10.1039/c7nr00810d

27. Mehdaoui, B.; Tan, R. P.; Meffre, A.; Carrey, J.; Lachaize, S.; Chaudret, B.; Respaud, M. *Phys. Rev. B* **2013**, 87, 174419. doi: 10.1103/PhysRevB.87.174419
28. Landi, G. T. *Phys. Rev. B* **2014**, 89, 014403. doi: 10.1103/PhysRevB.89.014403
29. Tan, R. P.; Carrey, J.; Respaud, M. *Phys. Rev. B* **2014**, 90, 214421. doi: 10.1103/PhysRevB.90.214421
30. Ruta, S.; Chantrell, R.; Hovorka, O. *Sci. Reports* **2015**, 5, 9090. doi: 10.1038/srep09090
31. Usov, N. A.; Serebryakova, O. N.; Tarasov, V. P. *Nanoscale Res. Lett.* **2017**, 12, 489. doi: 10.1186/s11671-017-2263-x
32. Usov, N. A.; Nesmeyanov, M. S.; Gubanova, E.M.; Epshtein, N. B. *Beilstein Journal of Nanotechnology* **2019**, 10 305–314. doi:10.3762/bjnano.10.29
33. Cēbers, A.; Ozols, M. *Phys. Rev. E* **2006**, 73(2). doi:10.1103/physreve.73.021505
34. Denisov, S. I.; Lyutyty, T. V.; Hänggi, P. *Phys. Rev. Lett.* **2006**, 97 (22). doi:10.1103/physrevlett.97.227202
35. Denisov, S. I.; Lyutyty, T. V.; Hänggi, P.; Trohidou, K. N. *Phys. Rev. B* **2006**, 74 (10). doi:10.1103/physrevb.74.104406
36. Yoshida, T.; Enpuku, K.; Dieckhoff, J.; Schilling, M.; Ludwig, F. *J. Appl. Phys.* **2012**, 111 (5), 53901. doi:10.1063/1.3688254.
37. Lyutyty, T. V.; Denisov, S. I.; Reva, V. V.; Bystrik, Y. S. *Physical Review E* **2015**, 92 (4). doi:10.1103/physreve.92.042312
38. Usadel, K. D. *Phys. Rev. B* **2017**, 95 (10). doi:10.1103/physrevb.95.104430.
39. Iszály, Z.; Lovász, K.; Nagy, I.; Márián, I. G.; Rácz, J.; Szabó, I. A.; Tóth, L.; Vas, N. F.; Vékony, V.; Nándori, I. *J. Magn. Magn. Mater.* **2018**, 466, 452–462. doi:10.1016/j.jmmm.2018.07.043
40. Dieckhoff, J.; Lak, A.; Schilling, M.; Ludwig, F. *J. Appl. Phys.* **2014**, 115 (2), 24701. doi:10.1063/1.4861032
41. Beković, M.; Trlep, M.; Jesenik, M.; Hamler, A. *J. Magn. Magn. Mater.* **2014**, 355, 12–17. doi:10.1016/j.jmmm.2013.11.045
42. Egolf, P. W.; Shamsudhin, N.; Pané, S.; Vuarnoz, D.; Pokki, J.; Pawlowski, A.-G.; Tsague, P.; de Marco, B.; Bovy, W.; Tucev, S.; Ansari, M. H. D.; Nelson, B. J. *J. Appl. Phys.* **2016**, 120 (6), 64304. doi:10.1063/1.4960406
43. Beković, M.; Trbušić, M.; Trlep, M.; Jesenik, M.; Hamler, A. *Advances in Materials Science and Engineering 2018* **2018**, 1–7. doi:10.1155/2018/6143607
44. Newman, J. J.; Yarbrough, R. B. *J. Appl. Phys.* **1968**, 39, 5566.
45. Newman, J. J.; Yarbrough, R. B. *IEEE Trans. Magn.* **1969**, 5 320.
46. Brezovich, I.A. *Med. Phys. Monogr.* **1988**, 16, 82.

47. Hergt, R.; Dutz, S. *J. Magn. Magn. Mater.* **2007**, 311, 187–192.
doi:10.1016/j.jmmm.2006.10.1156:
48. Brown, Jr., W. F. *Phys. Rev.* **1963**, 130, 1677-1686. doi: 10.1103/PhysRev.130.1677
49. Garcia-Palacios, J. L.; Lazaro, F. J. *Phys. Rev. B.* **1998**, 58, 14937-14958. doi:
10.1103/PhysRevB.58.14937
50. Scholz, W.; Schrefl, T.; Fidler, J. *J. Magn. Magn. Mater.* **2001**, 233, 296-304.
doi: 10.1016/S0304-8853(01)00032-4
51. Coffey, W. T.; Kalmykov, Yu. P.; Waldron, J. T. *The Langevin Equation*, 2nd ed.; World Scientific, Singapore, **2004**. doi:10.1142/5343
52. Coffey, W. T.; Kalmykov, Yu. P. *J. Magn. Magn. Mater.* **1996**, 164, 133.

Appendix

Based on the numerical results presented in Figure 1, the time dependence of the unit vectors $\vec{\alpha}$ and \vec{n} within the domains I and II in Figure 2 is assumed to be

$$\vec{\alpha}(t) = (\sin \theta_1 \cos(\omega t - \delta_1), \sin \theta_1 \sin(\omega t - \delta_1), \cos \theta_1); \quad (1^*)$$

$$\vec{n}(t) = (\sin \theta_2 \cos(\omega t - \delta_1 - \delta_2), \sin \theta_2 \sin(\omega t - \delta_1 - \delta_2), \cos \theta_2). \quad (2^*)$$

Here $\omega = 2\pi f$ is the given angular frequency of RMF in the plane XY. Spherical angles θ_1 and θ_2 describe the deviation of the vectors $\vec{\alpha}$ and \vec{n} from the XY plane. The angle δ_1 gives a constant phase shift between the vector $\vec{\alpha}$ and the RMF vector (1), whereas angle δ_2 gives a constant phase shift between the vectors $\vec{\alpha}$ and \vec{n} , respectively. Thus, the unknown variables of the problem are 4 time-independent angles, θ_1 , θ_2 and δ_1 , δ_2 .

First of all, it follows from Eqs. (1*), (2*) that the scalar product of unit vectors $\vec{\alpha}$ and \vec{n} does not depend on time

$$\xi = \vec{\alpha}(t) \cdot \vec{n}(t) = \sin \theta_1 \sin \theta_2 \cos \delta_2 + \cos \theta_1 \cos \theta_2. \quad (3^*)$$

Substituting Eqs. (1*), (2*) into Eq. (2), one finds that this equation is satisfied under the conditions

$$; \quad \cos \theta_1 = \xi \cos \theta_2; \quad (4^*)$$

$$\omega \sin \theta_2 = G \xi \sin \theta_1 \sin \delta_2. \quad (5^*)$$

Similarly, it can be shown that Eqs. (1*), (2*) also satisfy the Eq. (3) provided that the following relations are fulfilled

$$H_0 \sin \delta_1 = H_k \xi \sin \theta_2 \sin \delta_2, \quad (6^*)$$

$$\omega \sin \theta_1 = \gamma \cos \theta_1 (H_k \sin \theta_1 \sin^2 \delta_2 - H_0 \cos \delta_1). \quad (7^*)$$

Thus, the unknown angles $\theta_1, \theta_2, \delta_1, \delta_2$ are the solutions of the nonlinear set of equations (3*) - (7*).

As Figure 2 shows, at fixed RMF amplitude the first mode of motion exists at sufficiently low frequencies. It can be shown that if both unit vectors are in the same magnetic potential well, then their z - components are small and negative. Further we restrict ourselves to this case. The case when the unit vectors lie in opposite magnetic potential wells differs only in the signs of their z - components.

For the first mode of particle motion, the set of nonlinear equations (3*) - (7*) can be analyzed in the limit of relatively small frequencies. Let us introduce a small parameter $\chi = \omega/G$. In the limit $\chi \ll 1$ the equations (3*) - (7*) have the following solutions

$$\sin \delta_1 = \frac{H_k}{H_0} \chi + \dots; \quad \sin \delta_2 = \chi + \dots; \quad \theta_1 = \theta_2 = \frac{\pi}{2} + \frac{G}{\gamma H_0} \chi + \dots \quad (8^*)$$

Eqs. (8*) confirm that z-components of the vectors $\vec{\alpha}$ and \vec{n} are small and negative. This is characteristic of the regime of stationary particle motion in the domain I in Figure 2.

For the second mode of particle motion, the z components of the unit vectors are positive (if the vectors belong to the same magnetic potential well) and are of the order of unity. This case is realized at $H_0 < H_k$ with increasing frequency, $\omega/G \sim 1$, $\omega/G < 1$. If the angles θ_1 and θ_2 are small, the set of equations (3*) - (7*) allows a solution

$$\theta_1 = \theta_2 = \frac{H_0 G}{H_k \omega} \frac{1}{\sqrt{1 + (\omega/G - G/\gamma H_k)^2}}; \quad \sin \delta_1 = \frac{1}{\sqrt{1 + (\omega/G - G/\gamma H_k)^2}}; \quad \sin \delta_2 = \frac{\omega}{G}. \quad (9^*)$$

It is remarkable that the set of equations (3*) - (7*) also makes it possible to estimate analytically the boundaries between the domains I – III for various stable modes of particle motion shown in Figure 2. Note that equations (3*) - (5*) do not contain angle δ_1 . If we eliminate the variable ξ from equations (4*), (5*) using equation (3*), then we arrive at the relations

$$\cos \delta_2 = \frac{\cos \theta_1 \sin \theta_2}{\sin \theta_1 \cos \theta_2}; \quad \sin \delta_2 = \frac{\omega \sin 2\theta_2}{G \sin 2\theta_1}. \quad (10^*)$$

Using the basic trigonometric identity, one can express the angle θ_1 through the angle θ_2

$$\cos^2 \theta_1 = \frac{1}{2} \cos^2 \theta_2 \left(1 + \sqrt{1 - (2\omega/G)^2 \sin^2 \theta_2} \right). \quad (11^*)$$

Further, using equation (5*), one can eliminate the variable ξ from equation (8*) and obtain the equation

$$\sin \delta_1 = \frac{H_k \omega \sin^2 \theta_2}{H_0 G \sin \theta_1}. \quad (12^*)$$

Thus, the angles $\theta_1, \delta_1, \delta_2$ can be considered as functions of the angle θ_2 . Finally, for the angle θ_2 one obtains from equation (7*) the equation

$$\frac{\omega}{\gamma H_k} \sin \theta_1 = \cos \theta_1 \left(\frac{(\omega/G)^2 \sin \theta_1 \sin^2 2\theta_2}{\sin^2 2\theta_1} - \frac{H_0}{H_k} \cos \delta_1 \right). \quad (13^*)$$

Equation (13*) has a solution for $\cos \theta_2 < 0$, $\theta_2 \approx \pi/2$, which corresponds to the domain I in Figure 2. In addition, it also has a solution for $\cos \theta_2 > 0$, which corresponds to domain II in this figure. Analysis of the solutions of the equation (13*) for the first and second magneto- dynamic modes of particle motion makes it possible to establish the domains of the existence of these modes on the plane (f, H_0) . The latter are shown in Figure 3.